Intermetallics 18 (2010) 429–433

Contents lists available at ScienceDirect

Intermetallics

journal homepage: www.elsevier.com/locate/intermet

Phase relationships at 600 °C of the Yb–Pd–Sn system from 25 to 100 at.% Yb

M. Giovannini [a,b,*], R. Pasero [a], A. Saccone [a]

[a] Dipartimento di Chimica e Chimica Industriale, Università di Genova, Via Dodecaneso 31, I-16146 Genova, Italy
[b] LAMIA-INFM-CNR, Corso Perrone 24, I-16152 Genova, Italy

ARTICLE INFO

Article history:
Received 31 July 2009
Received in revised form
3 September 2009
Accepted 4 September 2009
Available online 21 October 2009

Keywords:
B. Phase diagram
B. Crystal chemistry of intermetallics

ABSTRACT

Phase equilibria in the Yb–Pd–Sn system at 600 °C were investigated in the range from 25 to 100 at.% Yb, employing scanning electron microscopy (SEM), electron probe micro-analysis (EPMA) and X-ray diffraction (XRD). The existence of five intermetallic compounds (YbPdSn, Yb_2Pd_2Sn, $YbPd_2Sn$, $YbPdSn_2$, $Yb_2Pd_3Sn_5$) was confirmed and three novel ternary phases were found. A few phases reveal a certain homogeneity range. In particular, Pd/Sn solubilities were found for $YbPd_2Sn$ and $YbPd_3$ compounds.

1. Introduction

In recent years a growing interest has been devoted to investigate strongly correlated electron systems, where hybridization of f-electrons and conduction electrons occurs. This fact in heavy fermion (HF) metals can cause a number of unusual low temperature features such as non-Fermi liquid (NFL) behavior [1], magnetic quantum phase transitions [2] and coexistence of magnetism and superconductivity [3]. Among the rare earths, a large number of these phenomena is found in Yb-and Ce-based HF compounds and alloys. It is worth mentioning that in comparison to the intensively studied Ce-based systems, much less studies were devoted to Yb compounds likely due to preparation difficulties associated with the high vapor pressure of Yb.

In this paper we present the results obtained in the investigation of the isothermal section at 600 °C of the Yb–Pd–Sn phase diagram. Our study was motivated by the interesting physical properties revealed in this system by some of the ternary compounds. In fact, whereas a certain number of Ce-based compounds showing superconductivity on the border of magnetism were already found [3], to date $YbPd_2Sn$ is one of the few examples of a Yb-based compound where superconductivity coexists with antiferromagnetism [4–7]. Yb_2Pd_2Sn is another compound of particular interest in the Yb–Pd–Sn system. In fact, possible occurrence of two quantum critical points (QCP) in Yb_2Pd_2Sn has been found either by applying pressure [8] than by doping with In [9,10].

The aim of this study is twofold. Chemical composition (as well as pressure and magnetic field) can play an important role in ground state properties of intermetallic compounds, and a relevant question to be addressed is whether a certain compound has a fixed composition or it forms in a homogeneity range [11]. Furthermore, our investigation is part of a systematic search of new intermetallic compounds of potential interest in the R–T–X (R = Ce, Yb, T = transition metal, X = p-block element) systems.

2. Literature data

2.1. Binary boundary systems

The assessed Yb–Sn phase diagram [12] is based on the work of Palenzona and Cirafici [13]. According to this assessment, of the five intermetallic compounds reported, two of them ($YbSn_3$ and Yb_2Sn) melt congruently, whereas YbSn, Yb_5Sn_4 and Yb_5Sn_3 form by peritectic reactions. In addition, two more phases were reported in recent papers, namely Yb_3Sn_5 [14] and $Yb_{36}Sn_{23}$[15]. The investigation of the Yb–Sn phase diagram is severely hampered by the high oxidability of the alloys in the central part of the system [12]. Moreover, a careful investigation on two of the phases reported in the assessment, namely Yb_3Sn_5 and Yb_5Sn_4, has shown that in the Yb–Sn system these phases are stabilized by hydrogen impurity [16]. As best compromise between literature data and observed results, in the present investigation of the Yb–Pd–Sn isothermal section at equilibria the following compounds have been accepted: $YbSn_3$, Yb_3Sn_5, YbSn, $Yb_{36}Sn_{23}$, Yb_2Sn.

The last assessment of the Yb–Pd phase diagram done by Okamoto [17] is based on the investigations done by Iandelli and Palenzona [18] by adding the compound $YbPd_7$ which forms by

* Corresponding author. Dipartimento di Chimica e Chimica Industriale, Università di Genova, Via Dodecaneso 31, I-16146 Genova, Italy. Tel.: +39 010 353 6648.
E-mail address: giovam@chimica.unige.it (M. Giovannini).

0966-9795/$ – see front matter © 2009 Elsevier Ltd. All rights reserved.
doi:10.1016/j.intermet.2009.09.002

Table 1
Crystallographic and micro-analysis data of selected Yb–Pd–Sn ternary alloys annealed at 600 °C.

Code N°	Alloy Nominal Comp.(at.%)	Phases[a]	EPMA at .% Yb,Sn[b]	Crystal structure	Lattice parameters (nm)			
					a	*b*	*c*	β (°)
1	$Yb_{45}Pd_{40}Sn_{15}$	τ_2	43; 17	tP10-Mo_2FeB_2	0.7589(2)		0.3635(1)	
		YbPd		cP2-CsCl	0.3449(1)			
2	$Yb_{25}Pd_{10}Sn_{65}$	$YbSn_3$	26.5; 73.5[c]	cP4- $AuCu_3$	0.4677(1)			
		τ_5	20; 49.5	oP40-$Yb_2Pt_3Sn_5$	0.736(2)	0.447(1)	2.639(6)	
		τ_4	24.3; 50	oS16-$MgCuAl_2$				
3	$Yb_{29}Pd_{37}Sn_{34}$	τ_1	33; 33.9	hP9-ZrNiAl	0.7587(2)		0.3762(1)	
		τ_3	25.8; 25	cF16-Cu_2MnAl	0.665(2)			
		τ_4	25; 49.2	oS16-$MgCuAl_2$				
4	$Yb_{28}Pd_{13}Sn_{59}$	τ_4	25;50	oS16-$MgCuAl_2$	0.4422(2)	1.110(5)	0.7383(2)	
		$YbSn_3$	27; 73	cP4-$AuCu_3$	0.4677(1)			
		Yb_3Sn_5	36; 64	oS32-Pu_3Pd_5				
5	$Yb_{38}Pd_{17}Sn_{45}$	τ_8	35; 45					
		YbSn	51; 49	tP2-AuCu	0.3536(1)		0.4320(1)	
		τ_7	33; 42					
		τ_1	33; 33.6	hP9-ZrNiAl	0.759(3)		0.376(1)	
6	$Yb_{35}Pd_{40}Sn_{25}$	τ_2	39.5; 19.8	tP10-Mo_2FeB_2	0.7577(2)		0.3637(1)	
		τ_3	26.6; 24.5	cF16-Cu_2MnAl	0.6654(2)			
		τ_1	33.3; 33.8	hP9-ZrNiAl				
7	$Yb_{52}Pd_{28}Sn_{20}$	Yb_2Sn	66.5; 33.5	hP6-$Co_{1.75}Ge$	0.536(1)		0.708(2)	
		YbPd	50.2	cP2-CsCl	0.3436(2)			
		τ_2	43; 17	tP10-Mo_2FeB_2	0.758(3)		0.363(2)	
8	$Yb_{30}Pd_{60}Sn_{10}$	τ_3	26; 21.5	cF16-Cu_2MnAl	0.6641(2)			
		$YbPd_3$	24.8; 3.1	cP4-$AuCu_3$	0.4050(2)			
		$YbPd_{1.63}$	36.8					
9	$Yb_{38}Pd_{47}Sn_{15}$	τ_2	39.7; 17.8	tP10-Mo_2FeB_2	0.7560(2)		0.3636(1)	
		Yb_3Pd_4	42.1; 57.9	hR42-Pu_3Pd_4	1.288(6)		0.566(2)	
		τ_3	25.5; 24.5	cF16-Cu_2MnAl	0.6654(2)			
10	$Yb_{21}Pd_{32}Sn_{47}$	τ_5	20; 50	oP40-$Yb_2Pt_3Sn_5$	0.732(2)	0.447(1)	2.645(6)	
		τ_4	25; 50	oS16-$MgCuAl_2$				
		τ_3	25; 25	cF16-Cu_2MnAl				
11	$Yb_{30}Pd_{65}Sn_5$	$YbPd_3$	24.4; 2.8	cP4-$AuCu_3$	0.4047(1)			
		$YbPd_{1.63}$	36.4					
		τ_3	27.2; 21	cF16-Cu_2MnAl	0.6646(2)			
12	$Yb_{45}Pd_{50}Sn_5$	YbPd	48.2	cP2-CsCl	0.3436(1)			
		Yb_3Pd_4	42.1	hR42-Pu_3Pd_4	1.287(4)		0.5650(2)	
		τ_2	42.2; 17	tP10-Mo_2FeB_2				
13	$Yb_{40}Pd_{32}Sn_{28}$	τ_6	42; 28	Orthorhombic				
		τ_1	33; 33	hP9-ZrNiAl	0.7577(2)		0.3758(1)	
		τ_2	40; 19	tP10-Mo_2FeB_2				
14	$Yb_{75}Sn_{25}$	Yb_2Sn	66; 34	hP6-$Co_{1.75}Ge$	0.5366(1)		0.7053(2)	
		Yb(β)	100	cF4-Cu	0.5489(2)			
15	$Yb_{60}Pd_{35}Sn_5$	YbPd	49.4	cP2-CsCl	0.3441(1)			
		Yb_5Pd_2	70	mS28-Mn_5C_2	1.63(5)	0.655(3)	0.763(3)	97.3(4)
		Yb_2Sn	66; 34	hP6-$Co_{1.75}Ge$				
16	$Yb_{78}Pd_{18}Sn_4$	Yb_3Pd	75.7	oP16-Fe_3C	0.7662(2)	0.968(3)	0.651(2)	
		Yb(β)	100	cF4-Cu	0.548(2)			
		Yb_2Sn	66; 34	hP6-$Co_{1.75}Ge$				
17	$Yb_{80}Pd_6Sn_{14}$	Yb(β)	100	cF4-Cu	0.548(2)			
		Yb_2Sn	67.5; 32.5	hP6-$Co_{1.75}Ge$	0.538(3)		0.707(3)	
		Yb_3Pd	77	oP16-Fe_3C	0.766(3)	0.968(4)	0.650(2)	
18	$Yb_{30}Pd_{26}Sn_{44}$	τ_7	25; 42	hP3- AlB_2	0.468		0.367	
		τ_1	33; 34	hP9-ZrNiAl	0.7585(2)		0.376(1)	
		τ_4	25; 50	oS16-$MgCuAl_2$	0.442(1)	1.109(4)	0.738(2)	
19	$Yb_{44}Pd_{28}Sn_{28}$	τ_6	44; 28	Orthorhombic	1.682	1.386	0.582	
		τ_1	33; 34	hP9-ZrNiAl				

[a] Reported in the order of their amount.
[b] All compositions are reported as atomic percent with accuracy ± 0.5 at.%.
[c] The composition was not measured because the phase was dispersed in a fine eutectic microstructure.

a peritectoid reaction at 449 °C [19]. All the seven compounds reported in the range from 25 to 100 at.% Yb, from Yb_3Pd to $YbPd_3$, have been accepted in this work.

Finally, the Pd–Sn system has been assessed by Massalski [20], and a range of intermetallic compounds, mostly forming peritectically, appear.

2.2. Yb–Pd–Sn ternary system

No constitutional data on phase equilibria for the Yb–Pd–Sn system are available in the literature.

A few Yb–Pd–Sn ternary compounds are known and they are briefly described in the following. The first ternary compound found in the Yb–Pd–Sn system was the equiatomic YbPdSn, which forms in low- and high-temperature modifications: YbPdSn (LT) of hexagonal ZrNiAl-type structure, and YbPdSn (HT) of orthorhombic TiNiSi-type structure, respectively [21]. The former structure exists for temperatures around 600 °C, whereas the latter, forming at around 1000 °C, is usually found in as-cast samples [22]. Measurements of magnetic susceptibility done by Kussman and co-workers [21] suggest that Yb is nearly divalent in YbPdSn (HT), whereas the value of the effective magnetic moment of 4.2 μB/Yb

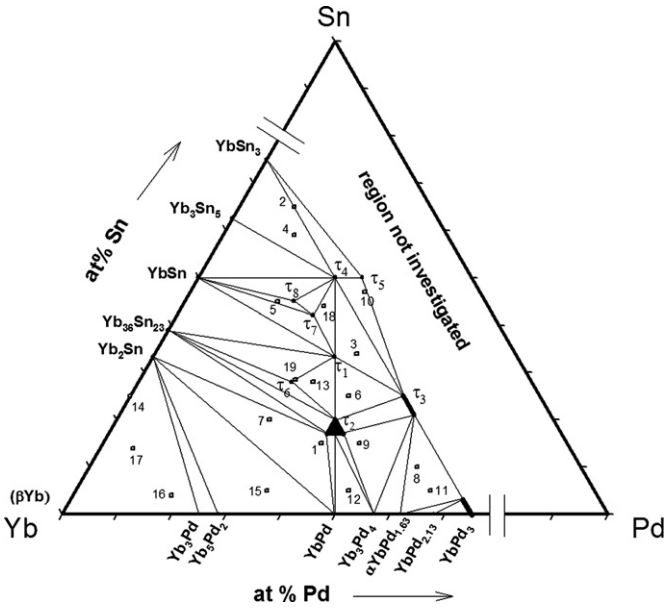

Fig. 1. Partial isothermal section at 600 °C of the Yb–Pd–Sn system based on the data collected. The region 0 < Yb < 25 at.% was not investigated. The ternary compounds are indicated by full points; the selected ternary alloys reported in Table 1 are marked by hollow squares.

atom in YbPdSn (LT) indicate that Yb in this modification is trivalent [21]. More recently, specific heat and magnetization measurements performed on YbPdSn (LT) revealed an antiferromagnetic order at $T_N = 0.2$ K [22].

$YbPd_2Sn$ is a peculiar Heusler compound (cubic Cu_2MnAl-type structure) where coexistence of superconductivity ($T_c = 2.3$ K) and simple antiferromagnetism ($T_N = 0.22$ K) occurs [4]. The antiferromagnetic order at 0.22 K was confirmed by neutron diffraction experiments [5], which reveal a commensurate antiferromagnetic structure with a propagation vector $k = [0,0,1]$. There are strong indications that the superconductivity in this compound is not heavy fermion in nature [6]. More likely, the cubic Pd sublattice is responsible for superconductivity, whereas the NaCl-type Yb–Sn sublattice plays an important role for the magnetic order [6].

Table 2
Crystallographic data of ternary compounds found in the partial isothermal section at 600 °C of the Yb–Pd–Sn system.

Phase/maximum homogeneity range	Pearson symbol/ prototype	Lattice parameters (nm)	Ref.
τ_1 YbPdSn (LT)	Hexagonal hP9-ZrNiAl	$a = 0.7580(1)$, $c = 0.3763(1)$ $a = 0.7587(2)$, $c = 0.3762(1)$	[21] [This work]
τ_2 Yb_2Pd_2Sn ($Yb_{39}Pd_{43}Sn_{18}$ to $Yb_{43}Pd_{40}Sn_{17}$)	Tetragonal tP10-Mo_2FeB_2	$a = 0.7580$, $c = 0.3639$ $a = 0.7577(2)$, $c = 0.3637(1)$ $a = 0.7589(2)$, $c = 0.3635(1)$[a] $a = 0.7560(2)$, $c = 0.3636(1)$[a]	[10] [This work] [This work] [This work]
τ_3 $YbPd_2Sn$ ($Yb_{25}Pd_{50}Sn_{25}$ to $Yb_{25}Pd_{53}Sn_{22}$)	Cubic cF16-Cu_2MnAl	$a = 0.6658$ $a = 0.6654(2)$ $a = 0.6641(2)$[a]	[26] [This work] [This work]
τ_4 $YbPdSn_2$	Orthorhombic oS16-$MgCuAl_2$	$a = 0.4424(2)$, $b = 1.1086(3)$, $c = 0.7384(2)$ $a = 0.4422(2)$, $b = 1.110(5)$, $c = 0.7383(2)$	[23] [This work]
τ_5 $Yb_2Pd_3Sn_5$	Orthorhombic oP40-$Yb_2Pt_3Sn_5$	$a = 0.734$, $b = 0.447$, $c = 2.643$ $a = 0.732(2)$, $b = 0.447(1)$, $c = 2.645(6)$	[24] [This work]
τ_6 $Yb_3Pd_2Sn_2$	Orthorhombic	$a = 1{,}682$, $b = 1.386$, $c = 0.582$	[This work]
τ_7 $YbPd_{0.7}Sn_{1.3}$	Hexagonal hP3-AlB_2	$a = 0.468$, $c = 0.367$	[This work]
τ_8 $Yb_{35}Pd_{20}Sn_{45}$	–	–	[This work]

[a] Related to off-stoichiometric compositions.

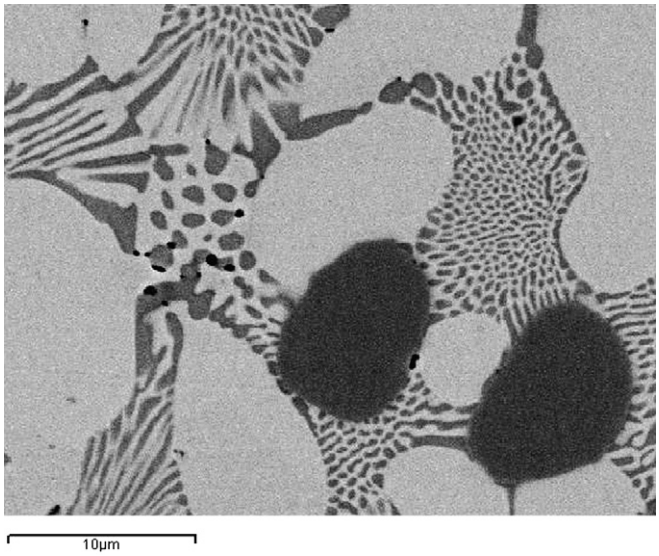

Fig. 2. SEM image (BSE mode, accelerating voltage: 20 kV) of the microstructure of $Yb_{30}Pd_{65}Sn_5$ (sample no. 11) annealed at 600 °C for 2 weeks and water quenched (bright phase, $YbPd_{1.63}$; dark phase, $YbPd_3$; grey phase, $YbPd_2Sn$; the eutectic shown in the figure is formed between $YbPd_{1.63}$ and $YbPd_2Sn$).

$YbPdSn_2$ crystallizes in the orthorhombic $MgCuAl_2$-type structure, a ternary ordered variant of Re_3B [23]. To date no data on physical properties are available for this compound.

$Yb_2Pd_3Sn_5$, crystallizing in the orthorhombic $Yb_2Pt_3Sn_5$-type, exhibits two crystallographically inequivalent Yb sites where both Yb atoms are in divalent states [24].

Finally, in previous investigations we have shown the existence of Yb_2Pd_2Sn with tetragonal Mo_2FeB_2-type structure [9,10]. From resistivity measurements under pressures of about 1 GPa performed on the paramagnetic Yb_2Pd_2Sn, it was observed that long range magnetic order is established, and above an upper pressure value of about 4 GPa magnetic order vanishes again [8]. This fact is a first indication of the possibility of two QCP induced by pressure within a single ordered compound. A similar behavior was obtained by doping Sn sites by In [9,10].

3. Experimental

The metals used were palladium (foil, 99.95 mass% purity, Chimet, Arezzo, Italy), tin (bar, 99.999 mass% purity, NewMet Kock, Waltham Abbey, UK) and ytterbium (pieces, 99.9 mass% purity, MaTecK, Jülich, Germany).

The samples, each with a total weight of 0.8–1 g, were prepared by weighing the proper amounts of elements by using an analytical balance. The elements were enclosed in small tantalum crucibles sealed by arc welding under pure argon, in order to avoid the loss of Yb with a high vapor pressure. The samples were melted in an induction furnace, under a stream of pure argon. To ensure homogeneity during the melting, the crucible were subjected to continuous shaking. All the alloys were then annealed in a resistance furnace at 600 °C for two weeks, and finally quenched in cold water.

Scanning electron microscopy (SEM) supplied by Carl Zeiss SMT Ltd, Cambrige, England, and electron probe micro-analysis (EPMA) based on energy-dispersive X-ray spectroscopy were used to examine phase equilibria and phase compositions. Smooth surfaces of specimens for microscopic observation were prepared by using SiC papers and diamond pastes down to 1 μm grain size. In most of

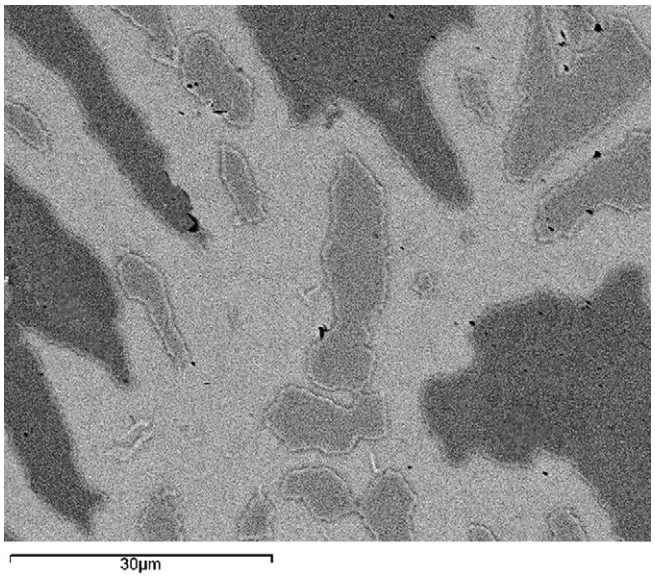

Fig. 3. SEM image (BSE mode accelerating voltage: 20 kV) of the microstructure of $Yb_{40}Pd_{32}Sn_{28}$ (sample no. 13) annealed at 600 °C for 2 weeks and water quenched (bright phase, $Yb_3Pd_2Sn_2$; dark phase, YbPdSn; grey phase, Yb_2Pd_2Sn).

the cases the compositional contrast among the phases was revealed in unetched samples by means of a backscattered electron detector (BSE). For the quantitative analysis an acceleration voltage of 20 kV was applied for 100 s, and a cobalt standard was used for calibration. The X-ray intensities were corrected for ZAF effects, using the pure elements as standards. No traces of tantalum contamination was found in the samples analysed.

X-ray diffraction (XRD) was performed on powder samples using the vertical diffractometer X'Pert MPD (Philips, Almelo The Netherlands), with Cu K_α radiation. In order to reduce particles size below ≈40 μm the specimens were ground in an agate mortar. Structure refinements of the XRD data were made by means of the program FULLPROF [25].

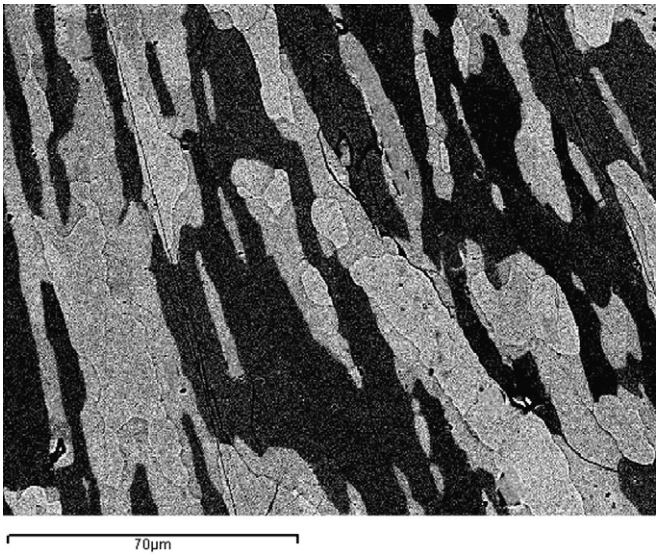

Fig. 4. SEM image (BSE mode, accelerating voltage: 20 kV) of the microstructure of $Yb_{30}Pd_{26}Sn_{44}$ (sample no. 18) annealed at 600 °C for 2 weeks and water quenched (bright phase, $YbPd_{0.7}Sn_{1.3}$; dark phase, $YbPdSn_2$; grey phase, YbPdSn).

Table 3
Structural parameters of Yb_2Pd_2Sn refined according to space group *P*4/*mbm* from X-ray diffraction data.

Atom	Site	*x*	*y*	*z*	Occ. [%]
Yb	4*h*	0.1724	0.6724	0.5000	100(2)
Pd	4*g*	0.3716	0.8716	0.0000	100(1)
Sn	2*a*	0	0	0	99(1)

Occ = occupation number, agreement R-Bragg factor $R_B = 8.9\%$, agreement R-structure factor $R_F = 6.3\%$.

4. Results

About fifty samples in the Yb–Cu–Sn system were prepared and characterized. The results obtained from EPMA and XRD analyses are listed in Table 1 for several alloys. The partial isothermal section at 600 °C, drawn on the basis of the results obtained, is reported in Fig. 1 and the crystal data relevant to the ternary compounds are listed in Table 2. In Figs. 2–4 the photomicrographs of selected samples are shown.

The isothermal section is characterized by the existence of eight ternary compounds (see Table 2). The crystal structures of the known ternary compounds have been confirmed. Two of the intermediate phases are not stoichiometric but exhibit a certain range of solid solubility. In particular, Pd/Sn substitution occur in τ_3, starting from the stoichiometric $YbPd_2Sn$ composition and extending up to 3–4% of Sn atoms substituted by Pd atoms. Disorder in $YbPd_2Sn$ occurs likely substituting Sn by the smaller Pd in the crystallographic site 4a of the space group *Fm*3 m which is fully occupied by Sn in the ordered compound. Correspondingly, lattice parameters slightly decrease from $a = 0.6654(2)$ to 0.6641(2) nm (see Table 2).

The solubility range of τ_2 is described by a more complex area. Starting from Yb_2Pd_2Sn, which is a fully ordered compound as demonstrated by the X-ray Rietveld refinement illustrated in Table 3 and Fig. 5, a slightly extending solid solution, depicted in Fig. 1 approximately as a triangular area, extends from 20 at.% up to 17–18 at.% Sn, and may originate from a more complex mechanism as in other R_2Pd_2X (R = rare earth X = In, Sn) compounds crystallizing in the tetragonal Mo_2FeB_2 [27, 28].

In this work YbPdSn has been always found crystallizing in the low temperature modification, hexagonal ZrNiAl-type, in agreement

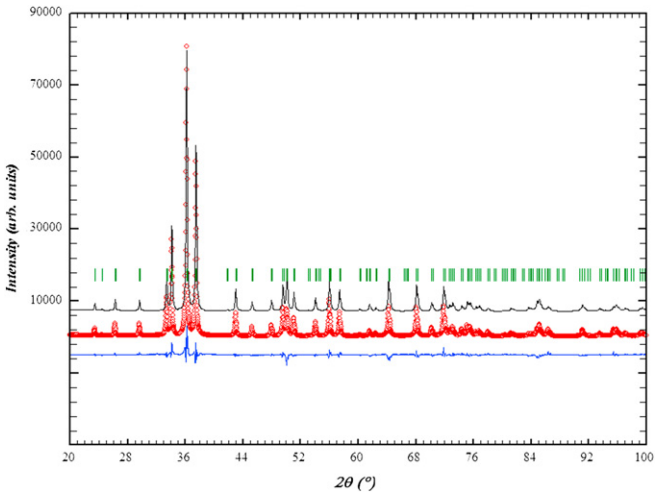

Fig. 5. The experimental X-ray diffraction power pattern of Yb_2Pd_2Sn compared with the calculated diffraction diagram. The experimental data are shown by the symbols, whereas the line through the data represents the results of the Rietveld refinement. A shift between the calculated and the experimental data was inserted. The lower curve is the difference curve. The ticks indicate the 2θ values of Mo_2FeB_2-type Bragg peaks.

with the temperature range of existence reported in the literature for this phase.

The compositions as well as the structures of the two orthorhombic ternary intermetallics $YbPdSn_2$ ad $Yb_2Pd_3Sn_5$ have been checked and the agreement between the data obtained and the literature data is very good, as shown in Tables 1 and 2.

As for the τ_6 phase, a sample prepared on the atomic composition 44 at.% Yb, 28 at.% Pd and 28 at.% Sn proved to be almost single phase (see sample N. 19 in Table 1) and the tentative formula $Yb_3Pd_2Sn_2$ was proposed. Powder diffraction peaks belonging to this phase were selected, and using the programs TREOR [29] and DICVOL [30] an orthorhombic cell was obtained [$a = 1.682$, $b = 1.386$, $c = 0.582$ nm].

Two new compounds τ_7 and τ_8 quite close in compositions ($Yb_{33}Pd_{25}Sn_{42}$ and $Yb_{35}Pd_{20}Sn_{45}$, respectively) were found in the region between 32–36 at.% Yb and 41–46 at.% Sn. The first compound, which can be written with the formula $YbPd_{0.7}Sn_{1.3}$, was successfully indexed with a hexagonal lattice with lattice parameters $a = 0.468$ nm, $c = 0.367$ nm, and it is compatible with the simple AlB_2 structure type (see Fig. 4 showing the appearance of this phase). This structure, in its disordered version where palladium and tin occupy the boron site, usually forms in small homogeneity ranges. Nevertheless, no homogeneity range of AlB_2-type seems to be present in the case of the Yb–Pd–Sn system. The second compound (τ_8) has a composition of 35 at.% Yb, slightly shifted compared to that of τ_7, and shows a more complex XRD pattern compared to that of τ_7. Attempts to obtain single phases failed for both compounds due to the closeness and the incongruent formation of τ_7 and τ_8, and any effort of indexing XRD pattern of τ_8 was unsuccessful.

All the binary phases were found to have negligible extensions into the ternary system, with the exception of the $YbPd_3$ phase extending up to 3 at.% Sn. As previously observed in the literature [12, 16], the binary phases in the central part of the Yb–Sn binary system are extremely oxidable and some of them are stabilized by impurities. As a consequence, micrographic examination was often very difficult and the determination of phase equilibria in the region close to the Yb–Sn binary boundary system was severely hampered. For this reason the phase equilibria in this region should be considered as tentative. Finally, more work is needed to complete the isothermal section and the crystal structures of the Yb–Pd–Sn intermetallics.

5. Summary

The 600 °C partial isothermal section of the ternary Yb–Pd–Sn system has been experimentally investigated and the tie-triangles have been drawn. Eight intermediate phases were found, and two of them exhibit a certain range of solubility. The crystal structures of the already known phases YbPdSn, Yb_2Pd_2Sn, $YbPd_2Sn$, $YbPdSn_2$ and $Yb_2Pd_3Sn_5$ were confirmed, and three new phases, $Yb_3Pd_2Sn_2$, $YbPd_{0.7}Sn_{1.3}$ and $Yb_{35}Pd_{20}Sn_{45}$ were found. The binary boundary phases do not extend into the ternary with the exception of $YbPd_3$, which exhibits a Pd/Sn solid solubility up to 3 at.% Sn.

References

[1] Bauer E, Berger ST, Gabani S, Hilscher G, Michor H, Paul CH, et al. Acta Physica Polonica B 2003;34:367.
[2] v Löhneysen H. J Magn Magn Mater 1999;200:532.
[3] See e.g. the following review Thalmeier P, Zwicknagl G, Stockert O, Sparn G, Steglick F. Superconductivity in heavy fermion compounds. Berlin: Springer; 2004.
[4] Kierstead HA, Dunlap BD, Malik SK, Umarji AM, Shenoy GK. Phys Rev B 1985;32:135.
[5] Dönni A, Fischer P, Fauth F, Convert P, Aoki Y, Sugawara H, et al. Physica B 1999;259–261:705.
[6] Aoki Y, Sato HR, Sugawara H, Sato H. Physica C 2000;333:187.
[7] Amato A, Roessli B, Fischer P, Bernhoeft N, Stunault A, Baines C, et al. Physica B 2003;326:369.
[8] Bauer E, Michor H, Muramatsu T, Kanemasa T, Kagayama T, Shimizu K, et al. J Optoelectron Adv Mater 2008;10:1633.
[9] Bauer E, Hilscher G, Michor H, Paul CH, Aoki Y, Sato H, et al. J Magn Magn Mater 2004;272–276:237.
[10] Bauer E, Hilscher G, Michor H, Paul CH, Aoki Y, Sato H, et al. J Phys Condens Matter 2005;17:S999.
[11] Giovannini M, Bauer E, Hilscher G, Michor H, Rogl P, Saccone A. J Optoelectron Adv Mater 2008;10:1595.
[12] Palenzona A, Cirafici S. J Phase Equilib 1991;12:482.
[13] Palenzona A, Cirafici S. J Less Common Met 1976;46:321.
[14] Manfrinetti P, Mazzone D, Palenzona A. J Alloys Compd 1999;284:L1.
[15] Leon-Escamilla EA, Corbett JD. Inorg Chem 1999;38:738.
[16] Leon-Escamilla EA, Corbett JD. Inorg Chem 2001;40:1226.
[17] Okamoto H. J Phase Equilibria 1993;14:770.
[18] Iandelli A, Palenzona A. Rev Chim Miner 1973;10:303.
[19] Takao K, Sakamoto Y, Araki T, Kohzuma H. J Alloys Compounds 1993;193:4.
[20] Massalski TB, Okamoto H, Subramanian PR, Kacprzak L, editors. Binary alloys phase diagrams. 2nd ed., vol. 1–3. ASM International; 1990.
[21] Kussman D, Pöttgen R, Kunnen B, Kotzyba G, Mullmann R, Mosel BD. Z Kristallogr 1998;213:356.
[22] Görlach T, Putselyk S, Hamann A, Tomanic T, Uhlarz M, Schappacher FM, et al. Phys Rev B 2007;76:205112.
[23] Kussman D, Pöttgen R. Z Naturforsch B 2001;56:446.
[24] Muro Y, Yamane K, Kim M, Takabatake T, Godart C, Rogl P. J Phys Soc Jpn 2003;72:1745.
[25] Rodriguez-Carvajal J. Physica B 1993;192:55.
[26] Malik SK, Umarji AM, Shenoy GK. Phys Rev B 1985;31:6971.
[27] Fourgeot F, Gravereau P, Chevalier B, Fournes L, Etourneau J. J Alloys Compounds 1996;238:102.
[28] Giovannini M, Michor H, Bauer E, Hilscher G, Rogl P, Fischer P, et al. Phys Rev B 2000;61B:4044.
[29] Werner PE, Eriksson L, Westdahl M. J Appl Crystallogr 1985;18:367.
[30] Boultif A, Louer D. J Appl Crystallogr 2004;37:724.